

Band insulator to Mott insulator transition in a bilayer Hubbard model

S. S. Kancharla and S. Okamoto

Materials Science and Technology Division, Oak Ridge National Laboratory, Oak Ridge, TN 37831

(Dated: October 30, 2018)

The ground state phase diagram of the half-filled repulsive Hubbard model in a bilayer is investigated using cluster dynamical mean field theory. For weak to intermediate values of Coulomb repulsion U , the system undergoes a transition from a Mott insulating phase to a metallic phase and then onto a band insulating phase as the interlayer hopping is increased. In the strong coupling case, the model exhibits a direct crossover from a Mott insulating phase to a band insulating phase. These results are robust with respect to the presence or absence of magnetic order.

PACS numbers: 71.10.-w, 71.10.Fd, 71.10.Hf, 71.27.+a, 71.30.+h, 71.45.Lr

Strong Coulomb interaction can localize electrons even in the absence of disorder to give rise to a gapped electronic state known as the Mott insulator. This state is of tremendous interest because upon addition of carriers it produces high temperature superconductivity and intriguing features such as a pseudogap in the normal state of the cuprates. Band insulators, on the other hand, lack the ability to conduct because they have either a filled or an empty band. The topic of transitions between band and Mott insulators has received considerable attention recently^{1,2,3,4,5,6,7}, because it provides a useful tool to understand the fundamental differences between the two states. Recent progress in the control of Fermionic atoms trapped in optical lattices adds to the experimental interest as it would be feasible to investigate the evolution of correlated ground states in a many body system. In a recent study, it was shown that the ground state of a Mott-insulating Haldane phase in a generalized Hubbard ladder can be connected *adiabatically* to a band insulating phase⁸. On the other hand, studies of the two dimensional ionic Hubbard model (IHM), which contains an alternating local potential $\pm\Delta$ on the A or B sublattice, find an intervening phase between the band and Mott insulating phases rather than a continuous evolution when the Coulomb repulsion is varied. Cluster dynamical mean field theory (CDMFT) calculations for the IHM at zero temperature suggest that the intervening phase is a bond-ordered insulator⁷ whereas finite temperature Quantum Monte Carlo techniques propose it to be a metal⁶.

Another theoretical model for the study of the band to Mott insulator crossover is the bilayer Hubbard model (BHM). The presence of copper-oxide bilayers, well described by doped Hubbard planes, in many of the high- T_c materials adds to the practical importance of studying the bilayer Mott system theoretically. The BHM was studied recently using Dynamical mean field theory (DMFT),⁵ and a smooth crossover between band and Mott insulators was observed. Since this study dealt with the infinite dimensional lattice, intralayer spatial correlations are absent. As a two-dimensional Hubbard model exhibits fundamentally different behavior from the infinite-dimensional Hubbard model, such as a pseudogap⁹ and d -wave superconductivity¹⁰ upon dop-

ing, a study incorporating the two-dimensional nature of the Hubbard planes in the BHM is expected to show richer physics.

In this work, we study the evolution of an antiferromagnetic (AF) Mott insulator into a band insulator as the interlayer hopping is varied in a bilayer Hubbard model at half-filling using cluster dynamical mean field theory¹¹. With interplane hopping set to t_{\perp} , the Hamiltonian for the bilayer Hubbard model can be written as

$$H = -t \sum_{\langle ij \rangle \sigma \alpha} (c_{i\sigma\alpha}^\dagger c_{j\sigma\alpha} + H.c.) + U \sum_{i\alpha} n_{i\downarrow\alpha} n_{i\uparrow\alpha} - t_{\perp} \sum_{i\sigma\alpha} c_{i\sigma\alpha}^\dagger c_{i\sigma(1-\alpha)}. \quad (1)$$

Here $\alpha = 0, 1$ labels the two Hubbard planes and U represents the onsite Coulomb repulsion. $c_{i\sigma\alpha}$ denotes the destruction operator at site i , with spin σ and on plane α . Chemical potential is chosen as $\mu = U/2$ so that the density is fixed to unity. In the limit $U \rightarrow 0$, it can be seen that the system goes from an uncorrelated metal to a band insulator at $t_{\perp} = 4t$ when the splitting between the bonding and antibonding bands produced by the two layers results in a finite gap. At large U and $t_{\perp} \rightarrow 0$, the system decouples into two Hubbard systems with a finite Mott gap and AF long range order in each layer.

In the recent study on the infinite-dimensional BHM, the two-plane system was reduced to two impurities embedded in a self-consistently determined bath⁵. For $t_{\perp} = 0$ the authors found a phase transition at $U = U_c$ from a metallic phase to a Mott insulating phase. As t_{\perp} is switched on, the Mott insulator (MI) evolves continuously into a band insulator (BI) with no sign of a phase transition. In what follows, we shall argue that in-plane spatial correlations provide a competing energy scale that is missing in the infinite dimension. Taking both intraplane and interplane spatial correlations into account within CDMFT we find that for $U < 8t$ as t_{\perp} is increased from zero the MI goes through a metallic phase before entering a band insulating phase. For larger values of U , the system undergoes a direct crossover from a MI to a BI without an intervening metallic phase.

CDMFT is a non-perturbative technique where the full many-body problem is mapped onto local degrees

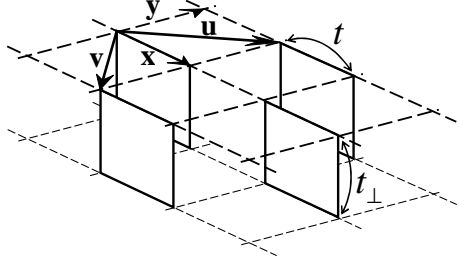


FIG. 1: Tiling the infinite bilayer with a 2×2 cluster

of freedom treated exactly within a finite cluster that is embedded in a self-consistent bath^{11,12}. It is a natural generalization of single-site DMFT¹³ to incorporate spatial correlations. The method has passed rigorous tests for the 1D Hubbard model where it compares well to exact solutions¹⁴ and has been applied to a variety of problems^{9,10}. The first step in the CDMFT method involves a tiling of the infinite lattice by a finite cluster. As seen in Fig. 1, we consider a 2×2 tiling cluster which includes both the in-plane and interplane hopping processes with a unit cell defined by the vectors $\mathbf{u} = \mathbf{x} + \mathbf{y}$ and $\mathbf{v} = \mathbf{x} - \mathbf{y}$. Using CDMFT, the BHM on the infinite lattice reduces to the cluster-bath Hamiltonian below, that is subject to a self-consistency condition:

$$H_c = \sum_{\langle \mu\nu \rangle \sigma} t_{\mu\nu} (c_{\mu\sigma}^\dagger c_{\nu\sigma} + H.c.) + U \sum_{\mu} n_{\mu\uparrow} n_{\mu\downarrow} + \sum_{m\sigma} \epsilon_{m\sigma} a_{m\sigma}^\dagger a_{m\sigma} + \sum_{m\mu\sigma} V_{m\mu\sigma} (a_{m\sigma}^\dagger c_{\mu\sigma} + H.c.). \quad (2)$$

Here, $\mu, \nu = 1, \dots, N_c$ denote indices labeling the cluster sites and $m = 1, \dots, N_b$ represent those in the bath. The self-consistent calculation proceeds by an initial guess for the cluster-bath hybridization $V_{m\mu\sigma}$ and the bath site energies $\epsilon_{m\sigma}$ to obtain the cluster Green's function $G_c^{\mu\nu}$. Applying the Dyson's equation, $\Sigma_c = \mathbf{G}_0^{-1} - \mathbf{G}_c^{-1}$, where \mathbf{G}_0 denotes the non-interacting Green's function for the Hamiltonian in Eq. (2), the cluster self-energy is obtained. Σ_c is then used in the self-consistency condition below to determine the local Green's function for the lattice:

$$\mathbf{G}_{loc}(z) = \frac{N_c}{2\pi^2} \int d\mathbf{P}_u d\mathbf{P}_v \frac{1}{z + \mu - t(\mathbf{P}_u, \mathbf{P}_v) - \Sigma_c(z)} \quad (3)$$

Here, \mathbf{P}_u and \mathbf{P}_v denote reciprocal lattice vectors conjugate to the spatial unit vectors \mathbf{u} and \mathbf{v} respectively, while $z = i\omega_n$ is the Fermionic Mastubara frequency. \mathbf{G}_{loc} can be used to obtain a new Weiss field, \mathbf{G}_0 , and consequently, a new set of $V_{m\mu\sigma}$ and $\epsilon_{m\sigma}$'s by means of a conjugate gradient minimization program to close the iterative loop. In this work, the Lanczos method is used to solve the cluster-bath Hamiltonian and we fix the bath size to $N_b = 8$. The Lanczos method can access both the strong and weak coupling regimes with equal ease and it is well suited to compute dynamical quantities directly

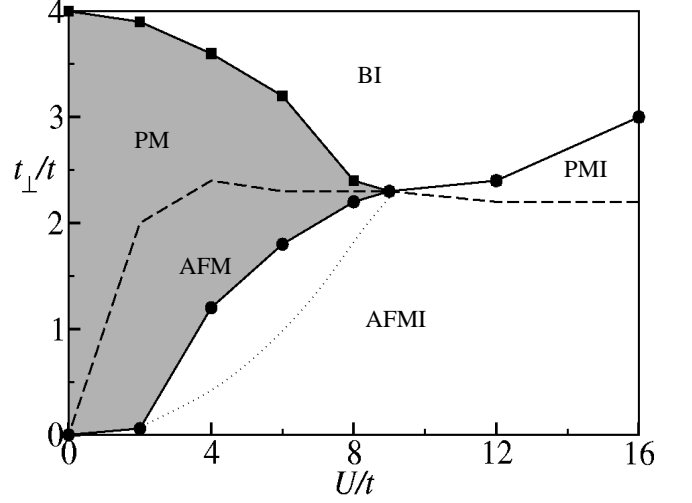


FIG. 2: Phase diagram for bilayer Hubbard model. Shaded portion shows the extent of the metallic region (paramagnetic metal (PM) and antiferromagnetic metal (AFM)) in the presence of magnetic order. Dashed line showing the magnetic phase boundary extends into the insulating region separating the paramagnetic Mott insulator (PMI) from the antiferromagnetic Mott insulator (AFMI). Suppression of magnetic order extends the metallic phase down to lower t_{\perp} shown by the dotted curve.

in real frequency. Rotational symmetries of the cluster on a square lattice, together with particle-hole symmetry at half-filling, reduce the number of bath parameters significantly. These bath parameters can depend on spin, allowing for symmetry breaking solutions. For details of the method, we refer to earlier work^{11,14}.

Let us start from the phase diagram with suppression of the magnetic order. Numerical results are shown in Fig. 2. We observe three states; a Mott insulating state at large U , a band insulating state at large t_{\perp} , and a metallic state in between. At $U = 0$, the BI and the metallic states are separated at $t_{\perp} = 4$ where the bonding and antibonding bands are separated. Critical t_{\perp} decreases with increasing U because the width of bonding and antibonding bands broaden due to correlation. Above $U = 12$, the BI and the MI states are adiabatically connected, but by close inspection of the charge gap, two regions are distinguishable; in the MI (BI) phase, Δ_c decreases (increases) with increasing t_{\perp} . Those features are consistent with the DMFT result on the infinite-dimensional BHM. In contrast to the infinite-dimensional case, the MI state extends down to small U and t_{\perp} in the two-dimensional case because of the intralayer spatial correlation, and the system passes through two phase transitions when increasing t_{\perp} at $0 < U < 12$. Thus, the two-dimensional BHM provides topologically distinct behavior as compared to the infinite-dimensional one. As will be discussed in detail below, this essential feature is not altered even by including the magnetic ordering.

We next investigate the magnetic properties of the bi-

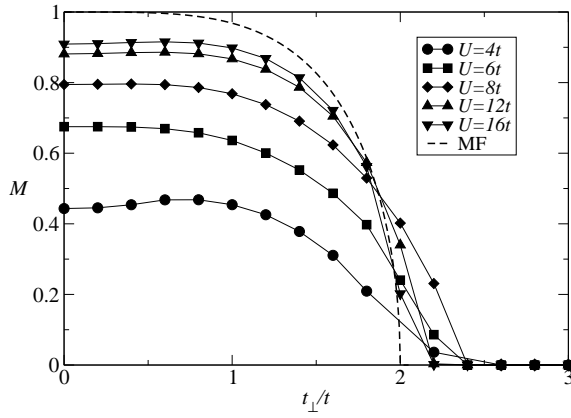


FIG. 3: Staggered magnetization a function of t_{\perp} for $U = 4t, 6t, 8t, 12t, 16t$

layer Hubbard model in detail. The staggered magnetization $M = n_{\uparrow} - n_{\downarrow}$ is plotted as the interplane hopping is varied in Fig. 3 for different values of U . At $t_{\perp} = 0$, the two planes are decoupled and the value of the staggered magnetization increases as U is increased, but quickly saturates to a value below unity because of quantum fluctuations. With increasing t_{\perp} , M stays fairly constant until $t_{\perp} = t$ and then drops rapidly to zero at about $t_{\perp} = 2t$. This value of $t_{\perp} = 2t$ is universal and does not depend on U for all $U > 8t$. The vanishing of the staggered magnetization at small U is caused by an increase in the effective bandwidth and a consequent reduction in the exchange coupling. In contrast, critical value $t_{\perp} \approx 2t$ at large U is due to the instability toward the formation of a local singlet. In this limit, the BHM is reduced to the $S = 1/2$ Heisenberg model with the intralayer exchange $J = 4t^2/U$ and the interlayer exchange $J_{\perp} = 4t_{\perp}^2/U$. By taking a dimer on the interlayer bond as a unit and introducing a mean-field decoupling on the intralayer bonds, critical exchange coupling for the transition from a Néel ordered state to an interlayer dimerized state is obtained as $J_{\perp} = 4J$ at $T = 0$, thus, $t_{\perp} = 2t$. Staggered magnetization $M = 2\langle S_z \rangle$ at $t_{\perp} < 2t$ is also computed. As shown with a dashed line in Fig. 3, this mean-field approximation to the bilayer Heisenberg model gives reasonable agreement with CDMFT at large U .

Next, we look at the local density of states for the BHM as a function of t_{\perp} at $U = 8t$ as shown in Fig. 4. As t_{\perp} is increased the Mott gap reduces till it closes completely at $t_{\perp} = 2t$ to give rise to a metallic state. The LDOS shows a clear quasiparticle peak along with the lower and upper Hubbard bands characteristic of Mott physics at $t_{\perp} = 2.4t$. Upon further increase of t_{\perp} we see that a gap opens abruptly to reveal a band insulating state. Increasing t_{\perp} in the band insulating phase causes the charge gap to grow monotonously unlike the Mott insulating phase where it reduces to zero. In Fig. 5 we plot the double occupancy and the charge excitation gap as a function of t_{\perp} for

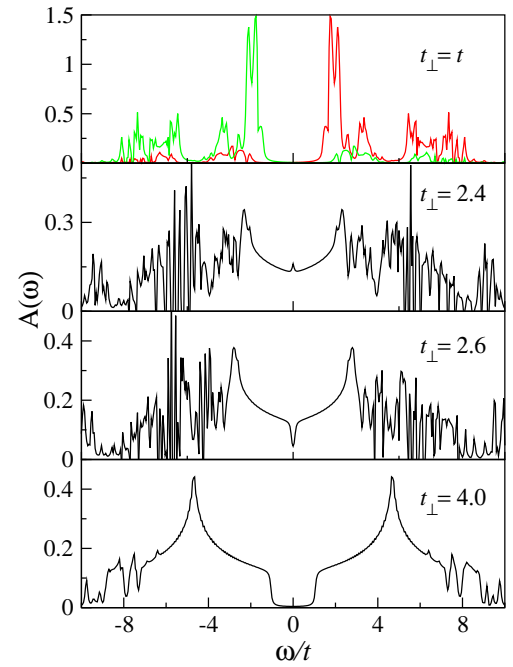


FIG. 4: Local density of states as t_{\perp} is varied at $U = 8t$. Spin-resolved density of states shown for $t_{\perp} = 1.0$ where magnetic order exists. Note the metallic state at $t_{\perp} = 2.4t$.

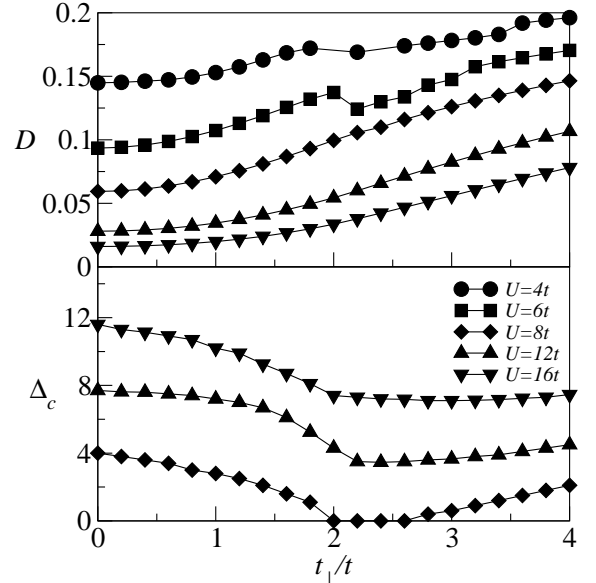


FIG. 5: Double occupancy (top panel) and charge excitation gap (bottom) as functions of t_{\perp} for various U indicated.

different values of U . For $U < 8t$, as t_{\perp} is increased in the Mott phase, the double occupancy rises and then shows a sharp kink as the system enters a metallic phase and also upon going into a band insulating phase. For larger values of U , as expected, the crossover from a Mott insulator to a band insulator is smooth with the double

occupancy showing no signs of a kink. The charge gap for large U shows a continuous decrease in the Mott phase but never goes to zero. The crossover to a band insulator around $t_{\perp} = 2t$ is easily identified by the increase in the charge gap with t_{\perp} .

The phase diagram for the bilayer Hubbard model that emerges for our calculation is shown in Fig. 2. We identify a region in the phase diagram which shows an intermediate metallic region, depicted by the shaded portion, which separates the band and Mott insulating phases. The width of the metallic region narrows with increasing U and eventually for $U > 8t$ there is a direct crossover from a band insulator to a Mott insulator. The magnetic phase boundaries are depicted by the dashed line which separates a antiferromagnetic metal from a paramagnetic metal. In the insulating portion of the phase diagram the magnetic phase boundary separates the antiferromagnetic Mott insulator (AFMI) from a paramagnetic Mott insulator (PMI). As we discussed earlier, emergence of intermediate metallic region separating BI and MI is a generic behavior in two-dimensional BHM independent of magnetic ordering.

In summary, we have obtained the zero temperature phase diagram of the bilayer Hubbard model at half-filling using cluster dynamical mean field theory. We computed the double occupancy and the local density of states as a function of the interlayer coupling t_{\perp} and the Coulomb repulsion U to identify a clear demarcation between a Mott insulating phase and a band insulating

phase as the interlayer coupling is varied. For weak to intermediate values of interaction ($U < 12t$), the Mott insulator at small t_{\perp} is separated from the band insulator at large t_{\perp} by an intermediate metallic phase. For $U > 12t$, there is a direct crossover from a Mott insulator to a band insulator as t_{\perp} is increased. This crossover is most clearly manifest in the behavior of the charge gap which first reduces in the Mott phase with increasing t_{\perp} and then increases in the band insulating phase. These results should be contrasted with the DMFT results for the infinite-dimensional model which always find a smooth crossover between the BI and MI states.⁵ These differences arise due to the presence of in-plane spatial correlations in the two-dimensional model stabilizing a Mott phase for all U at half-filling which is accessible by cluster DMFT. We completed the phase diagram by further allowing for magnetic order. The phase diagram is essentially unchanged, except that the onset of the metallic phase occurs at a larger value of t_{\perp} for a fixed value of U .

S.S.K acknowledges discussions with Achim Rosch. S.S.K. is supported by the LDRD program at Oak Ridge National Laboratory. This work is supported by the Division of Materials Sciences and Engineering, Office of Basic Energy Sciences, U.S. Department of Energy, under contract DE-AC05-00OR22725 with Oak Ridge National Laboratory, managed and operated by UT-Battelle, LLC.

¹ A. P. Kampf, M. Sekania, G. I. Japaridze and P. Brune, *J. Phys. Cond. Matter* **15** 5895 (2003).

² S. R. Manmana, V. Meden, R. M. Noack and K. Schonhammer, *Phys. Rev. B* **70**, 155115 (2004).

³ C. D. Batista and A. A. Aligia, *Phys. Rev. Lett.*, **92**, 246405 (2004).

⁴ A. Garg, H. R. Krishnamurthy and M. Randeria, *Phys. Rev. Lett.* **97**, 046403 (2006).

⁵ A. Fuhrmann, D. Heilmann, H. Monien, *Phys. Rev. B* **73**, 245118 (2006).

⁶ N. Paris, K. Bouadim, F. Hebert, G.G. Batrouni and R.T. Scalettar, *Phys. Rev. Lett.* **98**, 046403 (2007).

⁷ S. S. Kancharla and E. Dagotto, *Phys. Rev. Lett.* **98**, 016402 (2007).

⁸ F. Anfuso and A. Rosch, arXiv:cond-mat/0609051 (2006)

⁹ B. Kyung, S. S. Kancharla, D. Senechal, A.-M. S. Tremblay, M. Civelli and G. Kotliar, *Phys. Rev. B* **73**, 165114 (2006).

¹⁰ S. S. Kancharla, M. Civelli, M. Capone, B. Kyung, D. Senechal, G. Kotliar and A.-M. S. Tremblay, arXiv:cond-mat/0508205 (2005).

¹¹ G. Kotliar, S. Y. Savrasov, G. Palsson and G. Biroli, *Phys. Rev. Lett.* **87**, 186401 (2001).

¹² T. Maier, M. Jarrell, T. Pruschke and M. H. Hettler, *Rev. Mod. Phys.*, **77**, (2005).

¹³ A. Georges, G. Kotliar, W. Krauth and M. Rozenberg, *Rev. Mod. Phys.*, **13**, (1996).

¹⁴ C. J. Bolech, S. S. Kancharla, and G. Kotliar, *Phys. Rev. B* **67**, 075110 (2003); M. Capone, M. Civelli, S. S. Kancharla, C. Castellani, and G. Kotliar, *Phys. Rev. B* **69**, 195105 (2004).